Journal of Infrastructure Preservation and Resilience

RESEARCH Open Access

Fabrication and characterization of multiphase bituminous materials for cold region pavements

Di Wang[1], Augusto Cannone Falchetto[1*], Fan Zhang[1], Chiara Riccardi[2] and Yuxuan Sun[1]

Abstract

In this study, the low temperature creep properties of multiphase bituminous materials (binder, mastic, Fine Aggregate Matrix—FAM, and mixture) were experimentally evaluated, and the impact of size effect on FAM and mixture specimen was also assessed. First, the mix design of mastic and FAM was performed based on the reference mixture Asphalt Concrete (AC) 22 TS. The mathematical adaptation to the boundary sieve method was applied to calculate FAM gradation and binder content. Next, a preparation method was proposed to produce Fine Aggregate Matrix (FAM) in a laboratory environment, and scale-up slab samples were also fabricated for FAM and mixture specimens to evaluate the size effect phenomenon. Finally, three-point bending (3 PB) creep tests were conducted on the multiphase bituminous specimens with different dimensions at -6 °C, -12 °C, and -18 °C with a modified Bending Beam Rheometer (BBR) device and a dynamic loading machine, depending on the sample size. Results indicate that the creep stiffness of the FAM was close to mixtures and much higher than the one observed in binder and mastic. The proposed fabrication approach provides a satisfactory method for preparing a representative FAM phase in the mixture, while the air voids can be easily adjusted during the slab compaction procedure. This study supports the idea of using FAM to discriminate asphalt mixtures for cold regions. The correlation between up-scaled FAM and mixture specimens should be further investigated, including different mixture types and corresponding FAM.

Keywords Bituminous materials, Low temperature properties, Multiphase, FAM, 3 PB tests, Size effect

Introduction

Durable and climate-resilient roads are essential for the European infrastructure system [1]. This aspect is especially true for asphalt pavements since more than 90% of the European road network is surfaced with asphalt materials [2]. Extreme weather conditions like heat and cold waves are expected to occur more frequently due to global warming [3, 4]. As a result, asphalt roads must have superior failure resistance under various climatic circumstances. Asphalt roads constructed in cold regions such as the northern areas of Europe, America, and Asia are exposed to extremely low temperatures, frost, and freeze–thaw cycles, leading to different distresses [5–8], deteriorations of the overall functional performance and eventually resulting in shorter service life [3, 9]. Therefore, it is crucial to precisely evaluate the low temperature features of bituminous materials and comprehend how roads distress evolute.

Numerous studies have been conducted to evaluate bituminous materials' properties at low temperatures; for this purpose, several experimental techniques, protocols, and criteria have been developed, mainly for the binder and mixing phases. For asphalt binder, the three-point bending (3 PB) creep test with Bending Beam Rheometer

*Correspondence:
Augusto Cannone Falchetto
augusto.cannonefalchetto@aalto.fi
[1] Department of Civil Engineering, Aalto University, Rakentajanaukio 4, 02150 Espoo, Finland
[2] Department of Civil and Industrial Engineering, University of Pisa, 56122 Largo L. LazzarinoPisa, Italy

(BBR) [10] and the Direct Tension Tester (DTT) [11] were used to estimate the grading temperature and low temperature creep properties. Besides, the Asphalt Binder Cracking Device (ABCD) [12], developed during the NCHRP IDEA 99 project [13], can also be used to directly assess the potential low-temperature cracking in field-like conditions. In the recent past, the 4 mm plate-plate geometry was introduced for the Dynamic Shear Rheometer (DSR) as an alternative to BBR [14]. Several follow-up studies attempted to generate correlations between BBR and 4 mm DSR measurements and parameters [15–17], and promising results were obtained in the case of a specific grading range of PG [18]. Numerous tests can be used to evaluate the low temperature strength and fracture behavior of the asphalt mixture [3, 19]. For strength properties, the uniaxial tension stress test (UTST), the indirect tension tester (IDT), and the thermal stress restrained specimen test (TSRST) can be adopted. In contrast, the Disc-shaped compact tension (DCT), Semi-Circular Bending (SCB), and notched three-point bending (3 PB) tests can be used to evaluate the fracture response.

It is crucial to acknowledge the limitations of these experimental procedures even though they were proven to reasonably characterize bituminous materials at low temperatures. On the one hand, there are ongoing debates over whether binder tests can adequately capture the comparable performance of mixtures when accounting for the complex components of the composite. Initial macro cracking typically appears in the intermediate material phase, such as asphalt mastic/mortar [20–22]. On the other hand, preparing asphalt mixture specimens requires a significant investment in time, materials, and expensive compacting devices for large samples. The tests themselves are time- and energy-consuming. Furthermore, no single test can provide creep and fracture characterization of asphalt materials as this is also size-dependent at low temperatures [23, 24]. Combined tests are required to better understand the overall behavior of asphalt materials at low temperatures. Moreover, in the authors' previous studies [3, 25], it has been proven that bituminous materials, particularly asphalt mixtures, behave in a quasi-brittle manner at low temperatures. Hence, as a result, the materials' structure size may significantly affect their nominal strength. This condition raises the question of whether the relatively small BBR dimension mixture [24] and/or FAM sample can genuinely capture the low temperature behavior of the asphalt mixture.

Theoretical background

Several models have been proposed to represent asphalt mixtures over the years [26, 27]. Among these, Lackner et al. [28] introduced a multiscale/multiphase concept to describe the viscoelastic response of asphalt roads. Four scales/phases were identified: binder, mastic/mortar, Fine Aggregate Mixtures (FAM), and mixture, while the continuum scale/macro phase was defined for the road structure. In this study, this model was further developed and displayed in Fig. 1. For the lowest scale (asphalt binder phase), a characteristic length of a few µm represents clusters of asphaltenes distributed in the

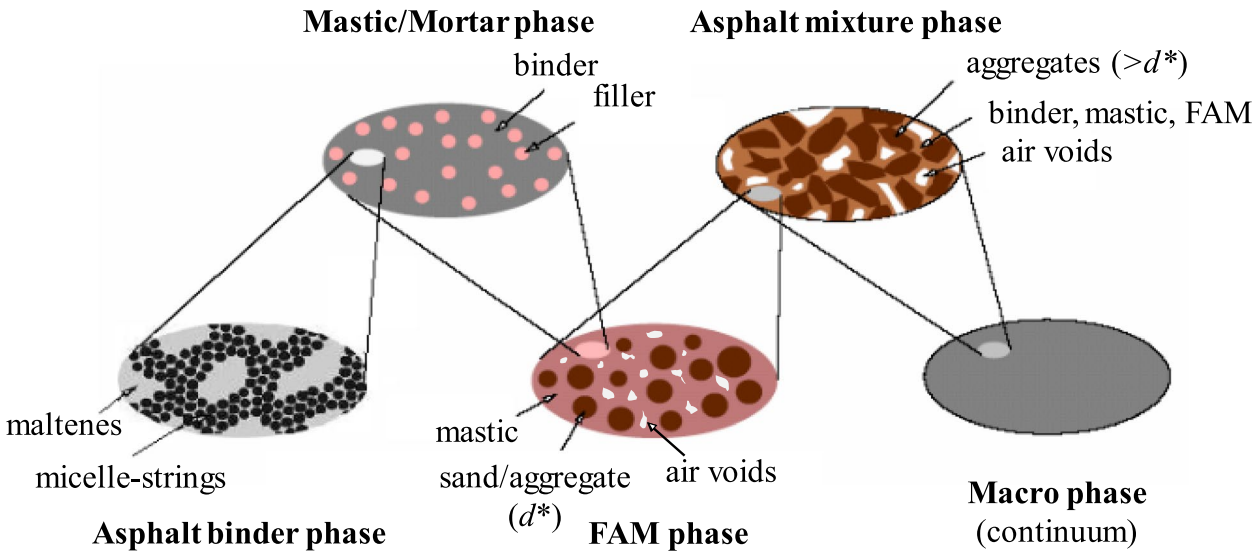

Fig. 1 Multiphase schematic of asphalt road materials based on [28]

maltene matrix. Filler smaller than a specific dimension is introduced for the next higher scale (mastic/mortar phase). For example, according to European standards [29], 63 μm is the critical diameter, while 75 μm is used in North America for defining the filler threshold. In the Fine Aggregate Mixtures (FAM) phase, the materials' component is asphalt binder, filler, fine aggregates, and air voids. The largest characteristic scale relies on the fine aggregates used. In the asphalt mixture phase, coarse aggregates were introduced, and the Nominal Maximum Aggregate Size (NMAS) was equal to the character scale. Mastic is typically considered an intermediate phase of bituminous material with generally consistent material properties that can be used to assess the overall performance of mixtures [30]. However, due to the lack of air voids, such material can not reflect the accurate response and behavior of the asphalt mixtures. Therefore, due to the air voids in the FAM, such a phase is considered more representative of asphalt mixtures and potentially could be used to estimate the mixture behavior [31]. It was validated that the FAM phases are where the initial thermal crack occurs and macro crack propagation starts [31, 32]. As a result, at low temperatures, FAM materials might be the phase potentially capable of discriminating the behaviors of corresponding mixtures [33, 34]. Furthermore, fewer material requirements and smaller specimen geometry lead to relatively inexpensive and fast tests for FAM. However, there are no uniform design standards for FAM. Previous studies found that FAM's design, including gradation, binder content, and air voids, could significantly influence its rheological behaviors. For instance, a 1% increase in binder content in FAM will result in a 20–35% reduction in the shear modulus, and a 1% decrease in air void will result in a 7% increase in the shear modulus [35, 36]; not to mention the maximum aggregate size and gradation. Hence, precisely determining the mix design of mixture-based FAM [36] is essential before characterizing its mechanical responses and rheological behaviors.

As previously stated, FAM consists of fine aggregate, filler, binder, and air voids. The fine aggregate defines the upper threshold size, while the fine aggregate and filler determine the gradation together. Fine aggregates are typically made up of particles with a sieving size smaller than 1.18 mm. Hence, 1.18 mm was commonly used as the maximum sieving size for designing FAM materials [35]. Alternatively, 4.00 mm, 2.36 mm, 2.00 mm, and 0.6 mm [37, 38] were also considered as upper threshold sieving sizes to design FAM. However, such a definition did not account for the gradation of mixtures. Considering that FAM could not exist independently of mixtures, a mixture gradation based, especially the Nominal Maximum Aggregate Size (NMAS), designing method should be applied for FAM. In this study, two concepts, primary and secondary control sieves, were introduced for this purpose. Based on Bailey's approach, the primary control sieve was designed with the assumption that only the largest aggregate could form the aggregate structure and function as a load-bearing component. Therefore, the upper threshold sieve size could be determined using the optimal aggregate size and packing theory [39]. The fine aggregate initial break sieve (D_{FAIB}), a function of the nominal maximum aggregate size, is the upper threshold sieve (NMAS). Following is a formula that may be used to calculate the $NMAS_{FAM}$:

$$FAIB = SCS = PCS \times 0.22 = NMAS \times 0.22^2 \quad (1)$$

where SCS is the secondary control sieve of the reference mixture, which is determined by multiplying the packing concept factor PCS by 0.22.

This strategy was further evolved in a follow-up study, and a protocol with nine calculation steps was proposed. The grading curve of the reference mixture was first introduced to establish the initial grading curve of FAM. Then, the fine aggregate and filler densities were considered to modify this grading curve. More detailed information can be accessed in this publication [31].

Several methods exist to determine the initial grading curve of FAM [40–43]. An empirical technique was initially applied directly to the FAM's binder content. A fixed binder concentration of 8% was suggested while considering a 10 μm binder film [40]. As previously stated, a constant component content in the design may ultimately result in no association between FAM and the reference mixtures. Hence, experimental methods were proposed, including the solvent extraction approach [41] and the ignition method [42], which ascertained the binder content in the FAM. However, poor repeatability and reproducibility were found in these two methods. In particular, limitations were observed for mixtures containing polymer-modified binders since it is challenging to physically separate FAM particles from the mixture. In addition, both methods were time-consuming, and the binder content could only be discovered after the extraction and recovery. Ng et al. [43] developed a novel calculation approach for the FAM's binder content utilizing the concept of surface area/specific surface to get over these limits (Ss). This approach was used under the hypothesis that FAM represented the mixture's fine matrix. As a result, the content of the binder in FAM should be directly proportional to that of the mixture. A series of formulations were developed to determine the FAM's reliable binder content (Pb_{FAM}). It should be emphasized that this technique was a crucial stage in the FAM design method that Underwood and Kim presented [31]. Therefore, this method was adopted to decide the

binder content. The ideal value for the air void is still up for dispute. Karki et al. [44] combined experimental work and numerical modeling to evaluate FAM materials with various air voids. It was discovered that 1% air void FAM samples show good agreement with the reference mixtures. As a result, the mix design method suggested by Underwood and Kim (2013) and 1% air voids were selected in this study.

Objective and research approach

This work experimentally characterized and modeled the low temperature creep properties and size effect on multiphase bituminous materials. First, the BBR dimension of four phases of bituminous materials—binder, mastic, Fine Aggregate Matrix (FAM), and mixture—were fabricated in the laboratory. The base layer dense-graded mixture, AC 22 TS, was selected as the reference material. Moreover, two different binder contents (one associated with the mixture and one with the FAM) were used in mastic to evaluate its effect. Then, scale-up specimens were fabricated for FAM and mixture materials. Next, a modified Bending Beam Rheometer (BBR) device and a dynamic loading machine were used to characterize the low temperature creep properties of multiphase bituminous materials at BBR size and scale-up dimensions, respectively. Finally, comparisons and discussions were conducted regarding the creep stiffness, S(60 s), relaxation properties, m-value, and Huet model parameters. Figure 2 provides a summary of the suggested research methodology.

Materials and experimental work

Fabrication of multiphase bituminous samples in different dimensions

In this study, a conventional German dense-graded base layer Asphalt Concrete (AC) mixture, AC 22 TS [45], was selected as the reference mixture. A 6% plain 50/70 binder [46], 4% air voids, and Gabbro aggregates (gradation shown in Fig. 3 in green) were used for this purpose. The roller sector compactor method [47] was used to produce mixture specimens. Then, the related specimen sizes, BBR dimension, 2 times scale-up BBR dimension, and 5 times scale-up BBR dimension were cut (Fig. 4). According to Eq. 1, the $NMAS_{FAM}$ is 1.084 mm based on AC 22 TS. Hence, 1 mm was selected based on the active European standard [45]. The initial grading curve of FAM (orange curve in Fig. 3) was established using the ideal aggregate size and packing principle [31]. The density of the filler and fine aggregates was then considered to adjust this curve (red curve in Fig. 3). The related binder content was determined to be 10.14% by weight, while a target air voids content of 1% [44] was selected.

There is no universal protocol for fabricating FAM specimens similar to the mix design. In earlier

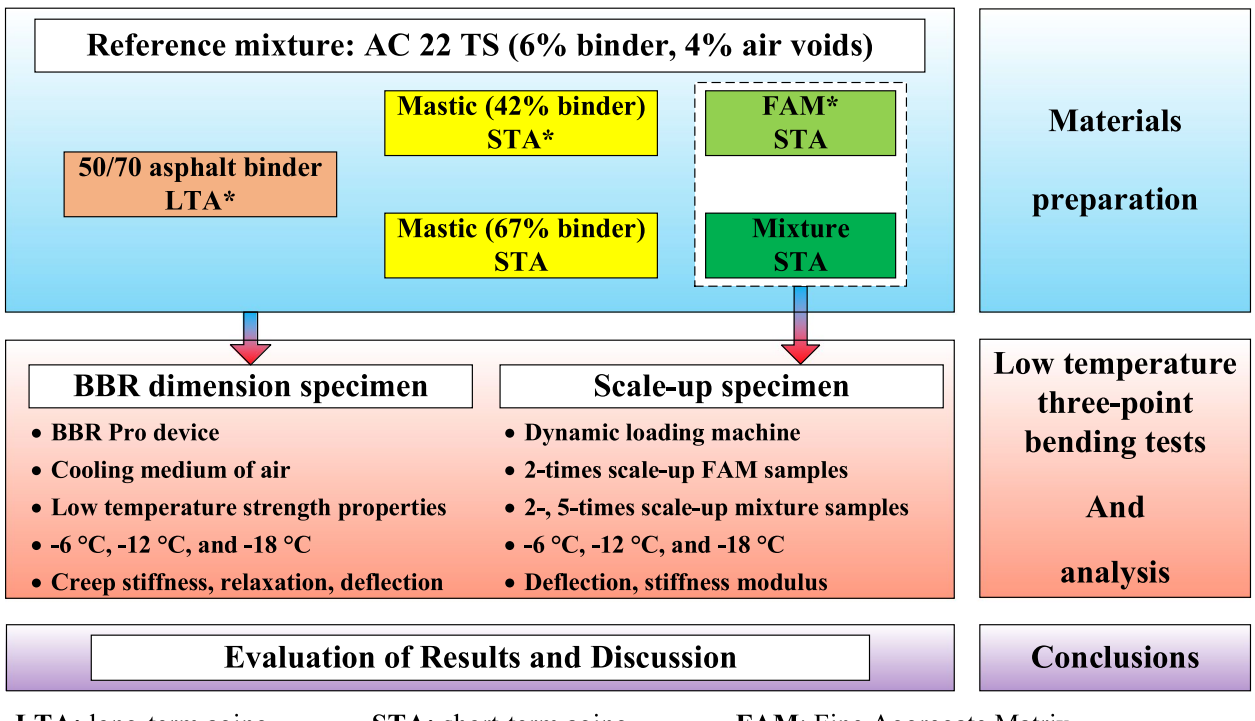

Fig. 2 Research approach

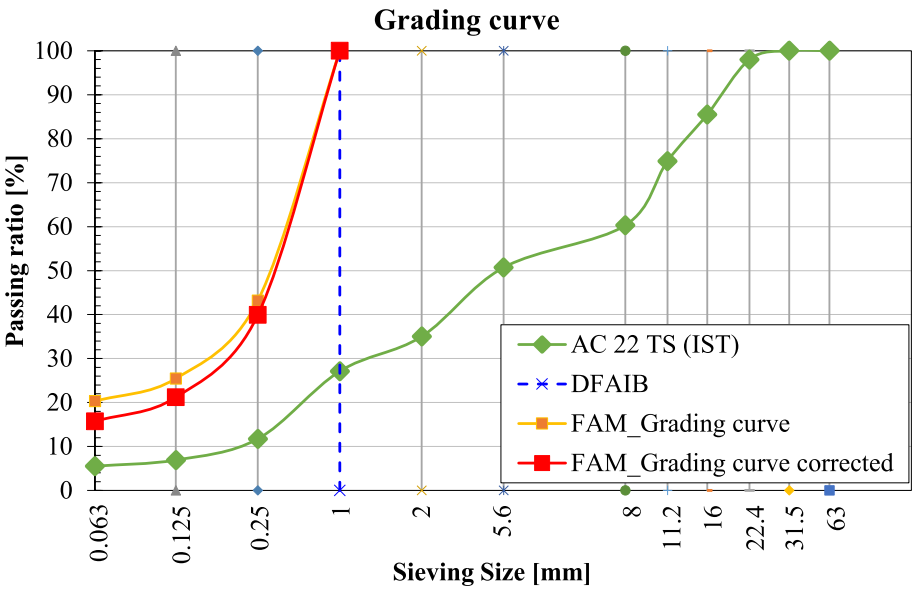

Fig. 3 Grading curve of AC 22 TS mixture and the related FAM

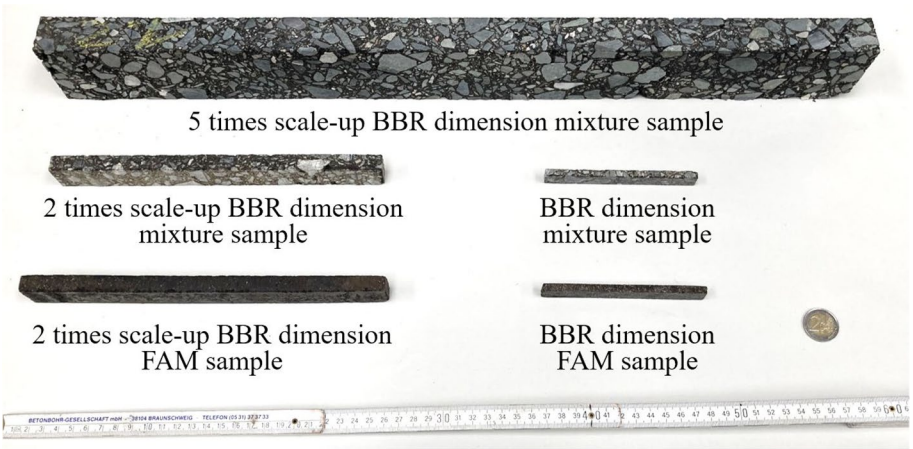

Fig. 4 BBR- and scale-up dimensions specimens of asphalt mixture and FAM materials

attempts, the Superpave Gyratory Compaction (SGC), Marshall compactor, and direct compaction procedures were used to manufacture FAM specimens [35]. A cylindrical FAM sample with a diameter of 100 mm or 150 mm can be prepared using the SGC procedure [48]. Then, cylindrical or prismatic specimens with a variety of diameters can be cored or sliced. Despite being frequently utilized in the mixture phase, the SGC method has drawbacks and complications in producing FAM, particularly when trying to reach the target air voids. Marshall compactor was used to create cylinder specimens with smaller sizes. However, this compactor imposes a pure impact loading action, completely disregarding the kneading effect brought on by the movement of the rollers [49]. Additionally, it was discovered that the samples from the Marshall compaction process had more brittle behaviors than the samples from the field cores [50], which will ultimately underestimate the low temperature properties. The direct compaction method for small-dimension cylindrical specimens (height range from 30 to 75 mm, and diameter from 12 mm to 12.5 mm) and prismatic specimens (length from 50 to 60 mm, width from 10 mm to 12.5 mm, while the height from 6 mm to 6.5 mm) has recently been proposed in addition to these two sample preparation techniques [51]. The loose components

were initially put into a specifically made mold, then compacted using fixed weighted loading units. With this approach, materials could be used most effectively, and fabrication time could be drastically decreased. The disadvantages of this approach, however, are also substantial. On the one hand, static loading cannot replicate the kneading effect during field compaction, similar to the Marshall compactor. On the other hand, the operators' considerable dependence on the compaction energy and air voids ultimately results in poor repeatability and comparability. As a result, these three techniques might not be appropriate for creating FAM specimens.

In this work, the FAM specimen was fabricated using the roller sector compactor method [47]. Pre-compaction and force-controlled main compression are the two primary processes during the compaction procedure. Both steps can replicate the rolling and kneading effects on construction sites in a laboratory environment. Additionally, the desired air voids can be easily and precisely achieved by flexibly adjusting the force and duration. This technique has been proven effective in manufacturing mixture specimens in various research [52, 53]. The current study relied on the parafilm-coated method [54] to validate the optimal compaction parameters to achieve 1% air voids. After the FAM slabs were fabricated, two specimen sizes, having BBR dimensions and 2 times scale-up BBR dimensions, were cut (Fig. 4).

The packing concept was utilized to determine the binder and filler contents for the formulation of mastic materials. The reference materials used were mixture and FAM, where the latter is rich in asphaltene, $mastic_{FAM}$ has a substantially larger binder content (67%) than $mastic_{mixture}$ (42%). The BBR geometry mastic samples were prepared using a method suggested in the authors' earlier studies [20, 55], and the short-term aged 50/70 binder was employed for this. The BBR geometry binder samples were prepared with the long-term aged 50/70 binders [10]. The components of each phase of bituminous materials are listed in Table 1. It should be noted that only the binder underwent the long-term aging condition while all the other materials were only short-term aged.

Low temperature *3PB tests*

Five multiphase BBR dimension specimens listed in Table 1 were utilized to assess their low temperature creep properties via a modified BBR device (Fig. 5 left). This apparatus was initially created for samples of BBR geometry mixtures at low temperatures [56]. The creep stiffness and relaxation characteristics could be accurately calculated with a higher loading force of 44 N, a longer loading duration of 1000 s, and air as the cooling medium. The follow-up study found better correlations between this technique and low temperature cracking in actual asphalt pavements [57]. Therefore, the same testing procedure was followed for the mixture test in this current study (Fig. 5 middle).

In an initial experiment, two higher loading forces, 2 N and 3 N, were attempted on FAM samples to find the optimal force. 3N was chosen based on sample response and deflection (Velasquez, 2009). Based on the authors' previous study [55], 1 N (980 ± 50 mN) was used for the mastic (Fig. 5 right) and binder samples. All materials

Table 1 Multiphase bituminous materials and component

BBR dimension beam samples	Mixture	FAM	Masticmixture	MasticFAM	Binder
Binder content [%]	6	10.14	42	67	100
Air voids [%]	4	1	-	-	-
Scale-up dimension beam samples	5 × Mixture	2 × Mixture	2 × FAM		
Binder content [%]	6	6	10.14		
Air voids [%]	4	4	1		

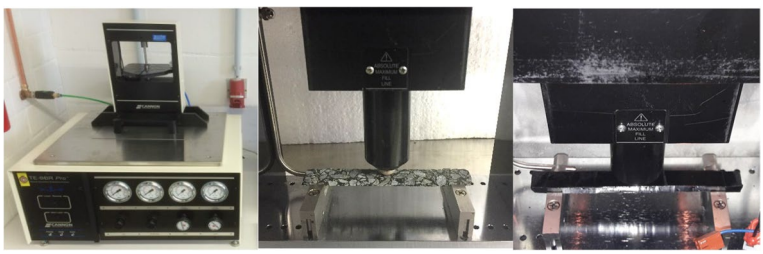

Fig. 5 BBR Pro device (left); BBR dimension samples set up: mixture sample (middle), mastic sample (right)

were tested for a single conditioning period of 1 h and a testing period of 1000 s. Three replicates were prepared along with three testing temperatures of -6 °C, -12 °C, and -18 °C. Creep stiffness, $S(t)$, and relaxation parameter (m-value) were measured and calculated, and then, the Huet model [58] was fitted to the experimental observations.

For scale-up samples, a dynamic loading machine was used for the low temperature 3 PB test. For comparison reasons, the samples were scaled up from the BBR geometry. In a previous study conducted by Velasquez [59], 2 times of BBR beam specimens were produced to evaluate the mixtures' low temperature creep properties via the 3 PB test, and 26 N was determined as the optimal loading force. Such a testing protocol was adopted for 2 times BBR mixture samples in this study (Fig. 6b). Considering the comparison purpose, a same-size FAM sample was produced. Based on the polynomial regression, a loading force of 22 N was set for 2 times the FAM sample (Fig. 6a). Due to the limitation of FAM slab size, the larger specimen was only designed and fabricated for mixtures. Considering the configuration of the loading machine, the largest specimen that can be set up was 5 times BBR beam geometry (600 mm span). Hence, such a size beam sample was fabricated and set on the loading device (Fig. 6c), and a loading force of 67 N was selected based on the polynomial regression. For the testing duration, two threshold criteria were used; the test ended either when it reached 1000 s or the deflection reached 1% [59]. Three replicators were applied for each material and temperature.

Results and analysis

3PB creep tests on BBR dimension specimens

The creep stiffness, S(60s), and relaxation characteristics, m-value (60s), were first calculated and fitted [10] for all five multiphase bituminous materials under three testing temperatures. Table 2 listed the results, and bar

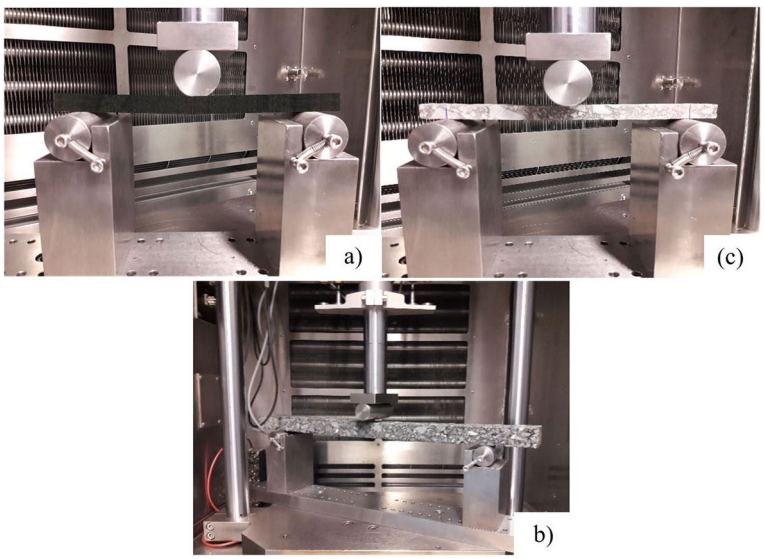

Fig. 6 3 PB tests configuration on dynamic loading machine: **a** 2 times scale-up FAM specimen; **b** 2 times scale-up mixture specimen; and **c** 5 times scale-up mixture specimen

Table 2 Comparison of S(60s) and m(60s) for multiphase BBR dimension samples

		Mixture	FAM	$\text{Mastic}_{\text{mixture}}$	$\text{Mastic}_{\text{FAM}}$	Binder
S (60 s) [MPa]	-6 °C	4183.3	2241.3	182.9	106.2	97.4
	-12 °C	8629.6	3206.8	480.0	268.0	194.8
	-18 °C	12,152.8	4893.9	1304.1	768.1	405.6
m (60 s) [-]	-6 °C	0.158	0.304	0.501	0.515	0.392
	-12 °C	0.108	0.246	0.421	0.403	0.300
	-18 °C	0.067	0.169	0.292	0.308	0.238

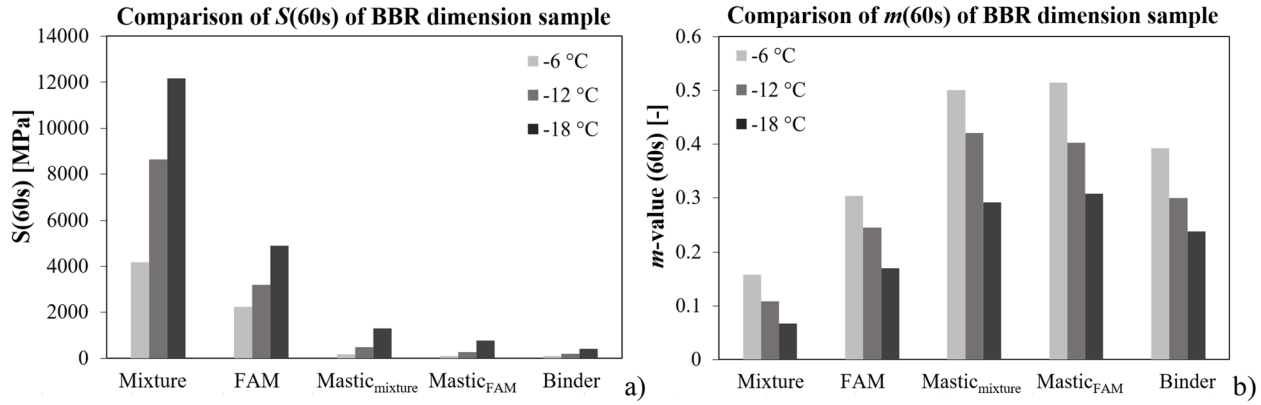

Fig. 7 Multiphase BBR dimension samples—results comparison: **a** *S* (60 s), and **b** *m*-value (60 s)

charts were plotted in Fig. 7. Since there are no critical values for multiple phases of bituminous materials except binder, only the changing trends were compared and discussed in this stage. It was observed that the differences in *S*(60s) are much larger than the ones in *m*(60s) among different phases; such differences were more remarkable at lower temperatures. For *S*(60s), the values increase with the phases. The results of FAM range four to ten times larger than mastic and binder phases; however, they are only about half as high as those obtained on the mixture. An increase of 25% in binder content in mastic leads to a more than 50% (52% to 57%) decrease in the creep stiffness results. It should be noted that the difference between $\text{Mastic}_{\text{FAM}}$ and binder, in comparison, is less than that between $\text{Mastic}_{\text{FAM}}$ and $\text{Mastic}_{\text{mixture}}$. Therefore, the creep results for FAM and mixes are comparable, whereas the features of the two mastics are comparable to those of the binder. In the case of *m-value* (60s) results, the differences between different phases and temperatures were much less remarkable. Interestingly, the results increased from binders to mastics while decreasing from mastic to mixture. Only limited differences were found between different binder contents in mastic, while the differences between FAM and lower phases were more remarkable. Therefore, FAM materials show very different behaviors from all other phases while closer to the mixture response than mastics and binders. Hence, FAM appears to exhibit a higher potential to represent mixtures' behavior to discriminate bituminous materials.

In addition to the standard low temperature creep parameters, a simple rheological model was introduced for further comparison. The Huet model [58], which consists of two parabolic elements and one spring, has been developed to assess the rheological responses of bituminous materials. This model was validated in different research and worked well in fitting low temperatures data [20, 55]. The following equation shows the expression for the creep compliance, $D(t)$:

$$D(t) = \frac{1}{S(t)} = \frac{1}{E_\infty}\left(1 + \delta\frac{(t/\tau)^k}{\Gamma(k+1)} + \frac{(t/\tau)^h}{\Gamma(h+1)}\right) \quad (2)$$

where,

$S(t)$ the creep stiffness;

E_∞ the glassy modulus for each material;

h, k exponents, commonly range from 0.08 ~ 0.3 (k) and 0.3 ~ 0.8 (h) in the relation of $0 < k < h < 1$;

δ dimensionless constant;

Γ the gamma function;

τ characteristic time, associated with the relaxation time of the material.

Figure 8 shows instances of the fitted and measured creep stiffness for all five multiphase samples performed at -6 °C, while all the fitted Huet parameters along with R^2 were provided in Table 3 for all conditions. It is clear that the Huet model reasonably describes the experimental creep stiffness. Hence, the fitted parameters can be utilized with confidence in the following discussion. Across all the different phases, it was found that the exponent parameters h and k were quite comparable. When considering the phases of simpler materials, smaller glass moduli, E_∞, characteristic times, τ, and higher form parameters, δ, were obtained. Unsurprisingly, such trends point to softer behavior in materials with simpler phases. However, a higher binder content in the mastic merely results in softer behavior and does not affect the glass modulus. In Fig. 9, two clusters were found, particularly for the evolution of the creep stiffness modulus over time. FAM's modulus is closer to those obtained in the mixture (Fig. 9 black dotted ellipse), while two mastic materials and the binder indicate similar performance (Fig. 9 red dotted ellipse). Table 3 shows that although E_∞, δ, and

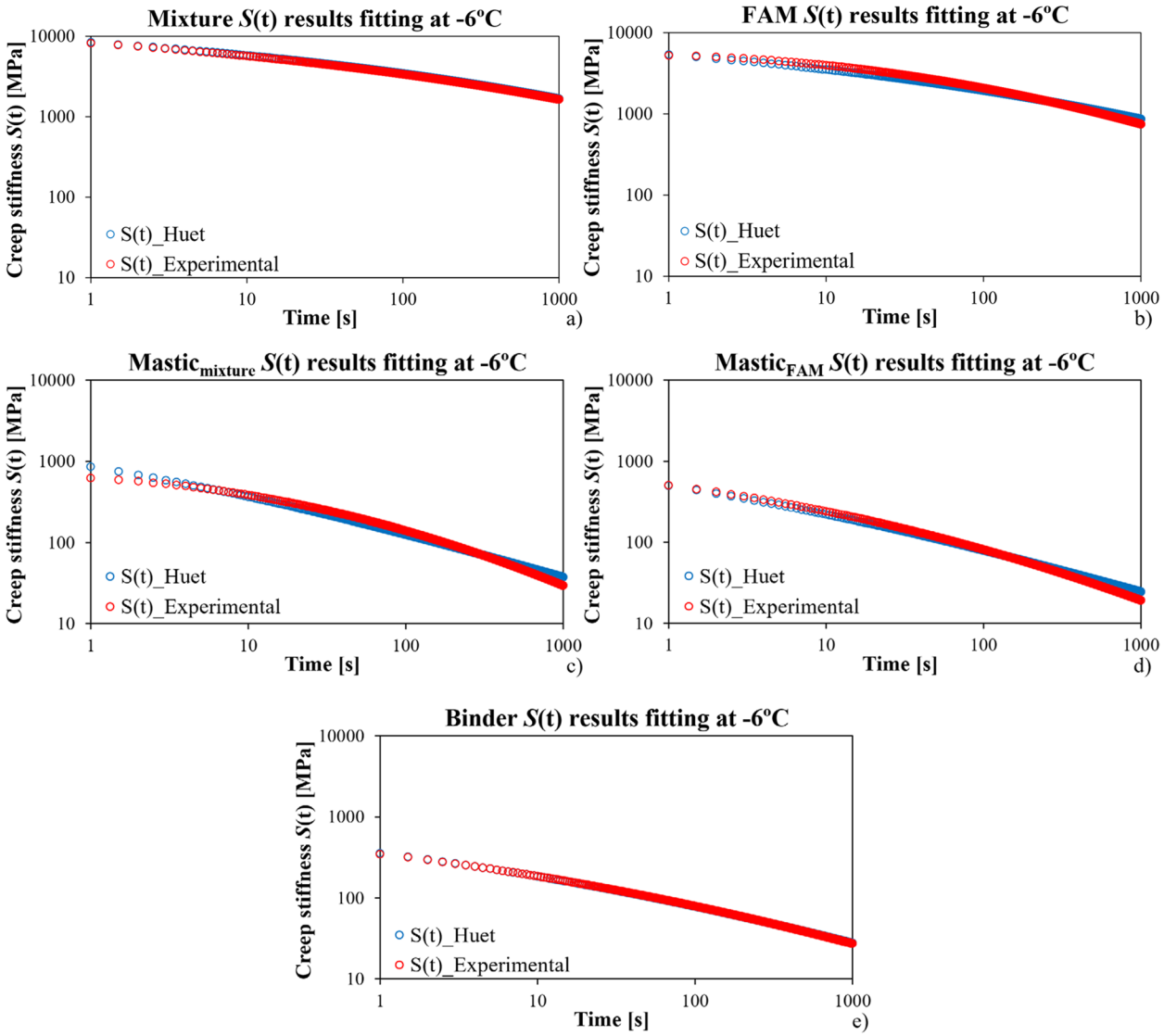

Fig. 8 Huet model fitting of *S*(*t*) for multiphase BBR dimension samples at *T* = -6 °C: **a** mixture, **b** FAM, **c** mixture-based mastic, **d** FAM-based mastic, and **e** binder

$\log(\tau_0)$ exhibited considerable variances within each cluster, the differences between the two clusters were more obvious than within cluster. However, this is not true for parameters *k* and *h*. In addition, the differences between the two clusters got smaller when the temperature became lower. Therefore, advanced statistical analysis is required to better understand the differences and correlations among different materials.

The grey relational analysis was conducted on the creep stiffness data to better understand the correlation among different materials. As shown in Fig. 7, the differences between creep stiffness are much more sensitive than the one in *m*-value. Hence, only measured creep stiffness results under different temperatures were used in this step; specifically, each replicate's stiffness result recorded at 8s, 15s, 30s, 60s, 120s, 240s, 480s, and 960s was used for this purpose. Accuracy testing was conducted first before the grey relational analysis [60]. The relative error test was selected since the mathematical process is simple and reliable. Fortunately, the relative error of the grey model is less than 5% in this study [60]. Therefore, the grey system models predicted results were considered to meet the requirements; results show the potential to reflect true development trends. Next, the grey absolute correlation degree ε_{0i} was calculated with the following equations:

Table 3 Huet model fitted parameter under all testing temperatures

Materials	Temperatures	E_∞ (MPa)	δ	k	h	log(τ_0)	R^2
Mixture	-6 °C	20,000	2.81	0.21	0.58	1.811	0.999
	-12 °C	20,000	2.81	0.21	0.58	2.354	0.997
	-18 °C	20,000	2.81	0.21	0.58	2.963	0.998
FAM	-6 °C	15,000	2.90	0.21	0.59	1.403	0.994
	-12 °C	15,000	2.90	0.21	0.59	1.922	0.991
	-18 °C	15,000	2.90	0.21	0.59	2.862	0.989
$Mastic_{mixture}$	-6 °C	5500	3.13	0.22	0.60	-0.575	0.964
	-12 °C	5500	3.13	0.22	0.60	0.436	0.995
	-18 °C	5500	3.13	0.22	0.60	1.733	0.996
$Mastic_{FAM}$	-6 °C	5500	3.94	0.22	0.61	-0.214	0.997
	-12 °C	5500	3.94	0.22	0.61	0.741	0.998
	-18 °C	5500	3.94	0.22	0.61	1.900	0.993
Binder	-6 °C	3000	5.91	0.23	0.64	-0.866	0.999
	-12 °C	3000	5.91	0.23	0.64	0.092	0.998
	-18 °C	3000	5.91	0.23	0.64	1.424	0.998

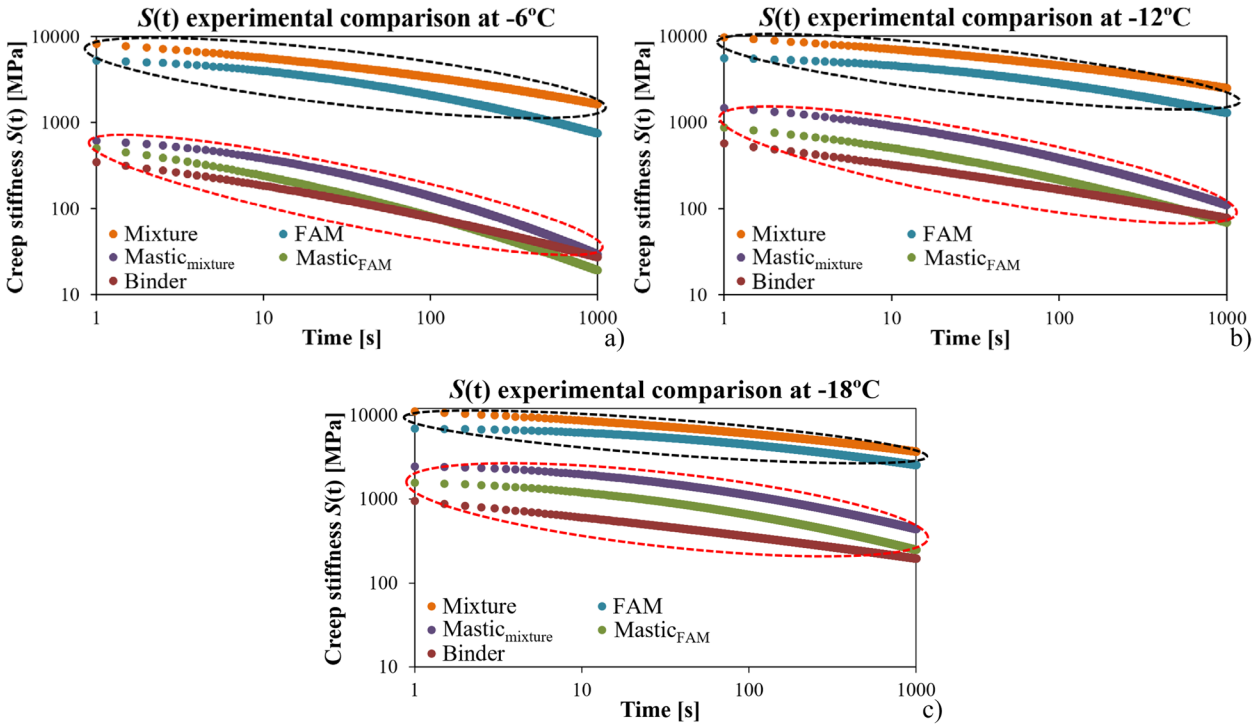

Fig. 9 Comparison of $S(t)$ results for multiphase BBR dimension samples: **a** -6 °C, **b** -12 °C, **c** -18 °C

$$\varepsilon_{0i} = \frac{1 + |S_0| + |S_i|}{1 + |S_0| + |S_i| + |S_i - S_0|} \tag{3}$$

$$|S_0| = \left| \sum_{k=2}^{n-1} x_0^0(k) + \frac{1}{2} x_0^0(n) \right| \tag{4}$$

$$|S_i| = \left| \sum_{k=2}^{n-1} x_i^0(k) + \frac{1}{2} x_i^0(n) \right| \tag{5}$$

$$|S_i - S_0| = \left| \sum_{k=2}^{n-1} \left(x_i^0(k) - x_0^0(k) \right) + \frac{1}{2} \left(x_i^0(n) - x_{i0}^0(n) \right) \right| \tag{6}$$

where,

$x_0^0(k), x_0^0(k)$ the value of the creep stiffness at the number k time (>0), k is the time serial number, while n is the total number of experimental time.

$x_i^0(k), x_i^0(k)$ the predicted 1-AGO (accumulated generation operation) sequence at the number k time (>0), k is the time serial number, while n is the total number of experimental times.

The gray absolute correlation degrees were calculated between each material using Eq. 3 and summarized in Table 4. The larger the value is, the better the correlation between the two materials is. The following classification was used to describe the relevance degree: excellent ($\varepsilon_{0i} > 0.9$), good ($0.8 < \varepsilon_{0i} \leq 0.9$), qualified ($0.7 < \varepsilon_{0i} \leq 0.8$), and unqualified ($\varepsilon_{0i} \leq 0.7$) [61]. In Table 4, it was found that under all three different temperatures, the degrees between Mixture and FAM are higher than 0.9 (excellent), which further supports the idea that FAM could be used to represent the related mixes response at low temperatures. Furthermore, it is not surprising that good correlations (between 0.8 and 0.9) were observed between two mastic materials ($Mastic_{mixture}$ vs. $Mastic_{FAM}$) and binder and the mastic with higher binder content ($Mastic_{FAM}$ vs. Binder). For all the other groups, unqualified correlations were found between most of them. This can be mainly attributed to the materials' components; both materials consist of binder, filler, aggregate, and air voids, so their mechanical response should be more similar. Moreover, in this study, the grading curve of FAM was determined based on the mixtures. Hence, it is not surprising that a better correlation was found between these two materials. For mastic, very limited differences were realized between mastic vs. FAM and mastic vs. binder; this may attributed to its intermediate phase between FAM and binder. In conclusion, the FAM sample proposed in this study indicates the potential to simulate and evaluate the response of the reference mixtures.

Table 4 Gray absolute correlation degrees between each material

Materials	-6 °C	-12 °C	-18 °C
Mixture vs. FAM	**0.9618**	**0.9471**	**0.9208**
Mixture vs. $Mastic_{mixture}$	0.5785	0.6479	0.6814
Mixture vs. $Mastic_{FAM}$	0.5481	0.5835	0.6231
Mixture vs. Binder	0.5305	0.5462	0.5604
FAM vs. $Mastic_{mixture}$	0.5850	0.6654	0.7275
FAM vs. $Mastic_{FAM}$	0.5521	0.5934	0.6463
FAM vs. Binder	0.5330	0.5517	0.5718
$Mastic_{mixture}$ vs. $Mastic_{FAM}$	**0.8265**	**0.8023**	**0.8215**
$Mastic_{mixture}$ vs. Binder	0.6940	0.6563	0.6578
$Mastic_{FAM}$ vs. Binder	**0.8166**	**0.8068**	**0.8154**

Correlation degrees higher than 0.8 are marked in bold

3PB creep tests on scale-up BBR dimension specimens

Figure 10 shows that most tests (except 2×BBR FAM) stopped at 1000 s at -12°C and -18°C; however, all tests at -6 °C finished earlier than 1000 s. This is because 1000 s or 1% deflection criteria were used for the testing duration. Hence, softer materials that reached 1% before 1000 s at higher temperatures were not unexpected. For all the conditions, at the beginning of the loading process, a peak deflection/creep stiffness was realized due to the contact load, then a smooth creep stiffness curve can be recorded (Fig. 10). The contact load of a minimum of 80 N was applied to ensure the loading unit touches the sample, which is higher than the applied loading force. The duration of such a period varied (ranging from 10 to 90 s). Hence, 60 s creep stiffness designed for BBR tests may not be suitable for such test protocol. Therefore, for the following analysis, the deflections over the entire testing duration were calculated and compared starting from $t = 100$ s. The calculated deflection rates are listed in Table 5.

In Table 5, it was found that the effect of contact load indicated greater influences on higher temperatures and simpler phases; overall, decreasing deflection rates were realized when reducing the temperature. In addition, fewer deflection steps were also found at low temperatures; this effect may be attributed to the high load-bear capability in stiffer materials. In Table 5, the deflection rates of the 5 times BBR mixture were way lower than the other 2 times BBR specimens; such differences became more significant with lower temperatures. The responses of 2 time BBR dimension mixture and FAM samples were closer, and the differences were mitigated at lower temperatures. Hence, for scale-up dimensions, in the same dimension scale, the low temperature response of FAM was similar to that of the mixtures already validated in the BBR dimension. In future research, larger FAM samples will be fabricated and evaluated to better understand the influence of size effect.

Summary and conclusions

This study used a modified Bending Beam Rheometer (BBR) test to investigate the low temperature strength properties of five different phases of bituminous materials, including mixture, Fine Aggregate Matrix (FAM), mixture-based mastic, FAM-based mastic, and asphalt binder. Furthermore assessed and discussed was the impact of the size effect phenomena on scaled-up BBR dimension samples. Testing temperatures of -6 °C, -12

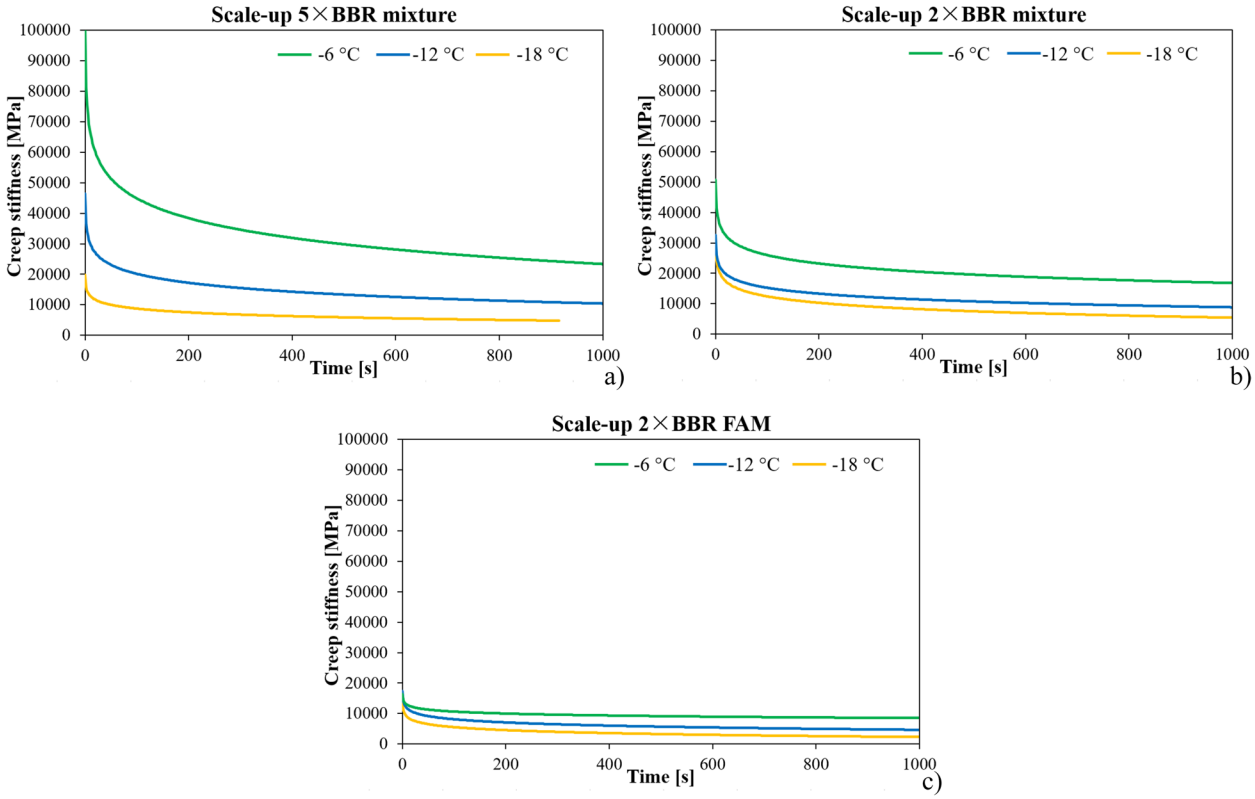

Fig. 10 Comparison of creep stiffness results for scale-up BBR dimension samples: **a**) 5 times mixture; **b**) 2 times mixture; **c**) 2 times FAM

Table 5 Comparison of the final deflection rate under different temperatures [unit: 1/100000%]

Scale-up beam samples	-6 °C	-12 °C	-18 °C
5×BBR mixture	0.94	0.24	0.01
2×BBR mixture	2.41	0.84	0.25
2×BBR FAM	4.72	1.30	0.31

°C, and -18 °C were applied for all materials. The resulting conclusions are as follows:

- FAM can be prepared using the designing and calculation method of Underwood and Kim (2013). Using different reference composites (mixture/mixes) will result in considerably different mastic materials based on the method's underlying assumptions.
- The roller sector compactor is a reliable and efficient device for preparing FAM specimens with precise air voids.
- When defining the mastic for the particular bituminous composite, careful consideration is required because the binder content in asphalt mastics greatly influences their low temperature behaviors (i.e., mixture, FAM, mortar).
- In the BBR dimension scale, FAM materials could produce outcomes equal to or comparable to mixes. Hence, when a solid analytical or model correlation can be established, FAM can potentially replace mixture testing by serving as a representative phase of the asphalt mixture at low temperatures.
- The responses of the 2 times BBR dimension FAM and mixed samples were comparable, particularly at lower temperatures, whereas the deflections of the 5 times BBR dimension mixture were significantly lower.

Although encouraging, the findings of this study still require further experimental validation. The current research effort is being expanded to investigate various sample sizes (for FAM and mixtures), size effect, loading force, and testing temperatures. Such a thorough examination may eventually advance our knowledge of how different phases of bituminous materials respond to low temperatures. Another aspect beyond the creep response is the different phases' fracture characteristics and failure behavior. These topics are part of upcoming research.

Authors' contributions
Di Wang and Augusto Cannone Falchetto designed and carried out the experimental work, Di Wang, Chiara Riccardi, and Fan Zhang contributed to the data analysis, and Chiara Riccardi and Yuxuan Sun made further recommendations. All the authors wrote the original manuscript together, reviewed the findings, and approved the final article.

Funding
Not applicable.

Availability of data and materials
Not applicable.

Declarations

Ethics approval and consent to participate
Not applicable.

Competing interests
The authors declare no competing interests.

Received: 18 April 2023 Revised: 13 September 2023 Accepted: 14 September 2023
Published online: 25 October 2023

References

1. Poulikakos LD, Papadaskalopoulou C, Hofko B et al (2017) Harvesting the unexplored potential of European waste materials for road construction. Resour Conserv Recycl 116:32–44. https://doi.org/10.1016/j.resconrec.2016.09.008
2. EAPA (2022) Asphalt in Figures 2021 (https://eapa.org/asphalt-in-figures/) Accessed 15 Sept 2022
3. Office JE, Chen J, Dan H, Ding Y et al (2021) New innovations in pavement materials and engineering: a review on pavement engineering research 2021. J Traffic Transp Eng 8(6):815–999. https://doi.org/10.1080/14680629.2019.1665089
4. Zhang K, Kevern J (2021) Review of porous asphalt pavements in cold regions: the state of practice and case study repository in design, construction, and maintenance. J Infrastruct Preserv Resilience 2(1):1–17. https://doi.org/10.1186/s43065-021-00017-2
5. Xu H, Guo W, Tan Y (2015) Internal structure evolution of asphalt mixtures during freeze–thaw cycles. Mater Des 86:436–446. https://doi.org/10.1016/j.matdes.2015.07.073
6. Cannone Falchetto A, Moon KH, Wang D et al (2018) Investigation on the cooling medium effect in the characterization of asphalt binder with the bending beam rheometer (BBR). Can J Civ Eng 45(7):594–604. https://doi.org/10.1139/cjce-2017-0586
7. Marasteanu MO, Cannone Falchetto A (2018) Review of experimental characterization and modelling of asphalt binders at low temperature. Int J Pavement Eng 19(3):279–291. https://doi.org/10.1080/10298436.2017.1347436
8. Wang D, Cannone Falchetto A, Riccardi C et al (2021) Investigation on the effect of physical hardening and aging temperature on low-temperature rheological properties of asphalt binder. Road Mater Pavement Des 22(5):1117–1139. https://doi.org/10.1080/14680629.2019.1665089
9. Wang T, Ma X, Li H et al (2021) Analysis methodology and assessment indices of vulnerability for asphalt pavement in cold regions. J Infrastruct Preserv Resilience 2(1):1–14. https://doi.org/10.1186/s43065-021-00028-z
10. AASHTO T313 (2022) Standard method of test for determining the flexural creep stiffness of asphalt binder using the Bending Beam Rheometer (BBR). American Association of State Highway and Transportation Officials
11. AASHTO T314 (2022) Standard Method of Test for Determining the Fracture Properties of Asphalt Binder in Direct Tension (DT). American Association of State Highway and Transportation Officials
12. Kim SS, Wysong ZD (1962) Kovach J (2006) Low-temperature thermal cracking of asphalt binder by asphalt binder cracking device. Transp Res Rec 1:28–35. https://doi.org/10.1177/036119810619620010
13. Kim SS (2007) Development of an Asphalt Binder Cracking Device," Final Report for NCHRP Highway IDEA Project 99, Transportation Research Board.
14. Sui C, Farrar MJ, Harnsberger PM et al (2011) New low-temperature performance-grading method: Using 4-mm parallel plates on a dynamic shear rheometer. Transp Res Rec 2207(1):43–48. https://doi.org/10.3141/2207-06
15. Lu X, Uhlback P, Soenen H (2017) Investigation of Bitumen Low Temperature Properties Using a Dynamic Shear Rheometer with 4mm Parallel Plates. Int J Pavement Res Technol 10:15–22. https://doi.org/10.1016/j.ijprt.2016.08.010
16. Riccardi C, Cannone Falchetto A, Wang D et al (2017) Effect of cooling medium on low-temperature properties of asphalt binder. Road Mater Pavement Des 18(sup4):234–255. https://doi.org/10.1080/14680629.2017.1389072
17. Wang D, Cannone Falchetto A, Riccardi C et al (2019) Investigation on the combined effect of aging temperatures and cooling medium on rheological properties of asphalt binder based on DSR and BBR. Road Mater Pavement Des 20(sup1):S409–S433. https://doi.org/10.1080/14680629.2019.1589559
18. Oshone MT (2018) Performance Based Evaluation of Cracking in Asphalt Concrete Using Viscoelastic and Fracture Properties. PhD Thesis, University of New Hampshire, Durham, USA
19. Cannone Falchetto A, Moon KH, Wang D et al (2018) Comparison of low-temperature fracture and strength properties of asphalt mixture obtained from IDT and SCB under different testing configurations. Road Mater Pavement Des 19(3):591–604. https://doi.org/10.1080/14680629.2018.1418722
20. Riccardi C, Cannone Falchetto A, Losa M et al (2018) Development of simple relationship between asphalt binder and mastic based on rheological tests. Road Mater Pavement Des 19(1):18–35. https://doi.org/10.1080/14680629.2016.1230514
21. Kim YS, Sigwarth T, Büchner J et al (2021) Accelerated dynamic shear rheometer fatigue test for investigating asphalt mastic. Road Mater Pavement Des 22(sup1):S383–S396. https://doi.org/10.1080/14680629.2021.1911832
22. Raab C, Arraigada M, Ibrahimi H (2022) Analysis of Low Temperature Cracking Behavior at Binder, Mastic and Asphalt Concrete Levels. In Proceedings of the RILEM International Symposium on Bituminous Materials: ISBM Lyon 2020. Springer International Publishing, pp. 255–261. https://doi.org/10.1007/978-3-030-46455-4_32
23. Moon KH, Cannone Falchetto A, Wang D et al (2017) Low-temperature performance of recycled asphalt mixtures under static and oscillatory loading. Road Mater Pavement Des 18(2):297–314. https://doi.org/10.1080/14680629.2016.1213500
24. Cannone Falchetto A, Moon KH, Wistuba MP (2017) Development of a simple correlation between bending beam rheometer and thermal stress restrained specimen test low-temperature properties based on a simplified size effect approach. Road Mater Pavement Des 18(sup2):339–351. https://doi.org/10.1080/14680629.2017.1305147
25. Cannone Falchetto A, Le JL, Turos MI et al (2014) Indirect determination of size effect on strength of asphalt mixtures at low temperatures. Mater Struct 47:157–169. https://doi.org/10.1617/s11527-013-0052-2
26. Underwood B (2011) Multiscale constitutive modeling of Asphalt concrete. Dissertation, North Carolina State University, Raleigh, USA
27. Nie F, Chow CL, Lau D (2022) A review on multiscale modeling of asphalt: development and applications. Multiscale Sci Eng 4(1–2):10–27. https://doi.org/10.1007/s42493-022-00076-x
28. Lackner R, Spiegl M, Blab R (2005) Is the low-temperature creep of asphalt mastic independent of filler shape and mieralogy?Arguments from multiscale analsysis. J Mater Civ Eng 17(5):485–491. https://doi.org/10.1061/(ASCE)0899-1561(2005)17:5(485)
29. EN 12697–2 (2015) Bituminous mixtures - Test methods - Part 2: Determination of particle size distribution. European Committee for Standardization
30. Miller C, Vasconcelos KL, Little DN et al (2011) Investigating aspects of aggregate properties that influence asphalt mixtures performance. Research Report DTFH61–06-C-00021. Texas A&M University and University of Texas at Austin, College Station and Austin.
31. Underwood BS, Kim YR (2013) Effect of volumetric factors on the mechanical behavior of asphalt fine aggregate matrix and the

relationship to asphalt mixture properties. Constr Build Mater 49:672–681. https://doi.org/10.1016/j.conbuildmat.2013.08.045
32. Haghshenas H, Nabizadeh H, Kim YR et al (2016) Research on high-rap asphalt mixtures with rejuvenators and WMA additives. Nebraska Department of Transportation Research Reports.
33. Im S, Ban H, Kim YR (2014) Characterization of mode-I and mode-II fracture properties of fine aggregate matrix using a semi-circular specimen geometry. Constr Build Mater 52:413–421. https://doi.org/10.1016/j.conbuildmat.2013.11.055
34. Le JL, Hendrickson R, Marasteanu MO et al (2018) Use of fine aggregate matrix for computational modeling of low temperature fracture of asphalt concrete. Mater Struct 51(6):152. https://doi.org/10.1617/s11527-018-1277-x
35. Suresha SN, Ningappa A (2018) Recent trends and laboratory performance studies on FAM mixtures: a state-of-the-art review. Constr Build Mater 174:496–506. https://doi.org/10.1016/j.conbuildmat.2018.04.144
36. Enríquez-León AJ, de Souza TD, Aragão FTS et al (2021) Characterization of the air void content of fine aggregate matrices within asphalt concrete mixtures. Constr Build Mater 300:124214. https://doi.org/10.1016/j.conbuildmat.2021.124214
37. Dai Q, You Z (2007) Prediction of creep stiffness of asphalt mixture with micromechanical finite-element and discrete-element models. J Eng Mech 133(2):163–173. https://doi.org/10.1061/(ASCE)0733-9399(2007)133:2(163)
38. Freire RA, FAL Babadopulos L, TF Castelo Branco V et al (2017) Aggregate maximum nominal sizes' influence on fatigue damage performance using different scales. J Mater Civ Eng 29(8):04017067. https://doi.org/10.1061/(ASCE)MT.1943-5533.0001912
39. Vavrik WR, Pine WJ, Huber G et al (2001) The bailey method of gradation evaluation: the influence of aggregate gradation and packing characteristics on voids in the mineral aggregate (with discussion). J Assoc Asphalt Paving Technol 70.
40. Kim YR, Little DN, Lytton RL (2003) Fatigue and healing characterization of asphalt mixtures. J Mater Civ Eng 15(1):75–83. https://doi.org/10.1061/(ASCE)0899-1561(2003)15:1(75)
41. Coutinho RP (2012) Utilização da parte fina de misturas asfálticas para avaliação do dano por fadiga. Master Thesis. Universidade Federal do Ceará, Fortaleza, Brazil. (in Portuguese)
42. Sousa P, Kassem E, Masad E et al (2013) New design method of fine aggregates mixtures and automated method for analysis of dynamic mechanical characterization data. Constr Build Mater 41:216–223. https://doi.org/10.1016/j.conbuildmat.2012.11.038
43. Ng AKY, Vale AD, Gigante AC et al (2018) Determination of the binder content of fine aggregate matrices prepared with modified binders. J Mater Civ Eng 30(4):04018045. https://doi.org/10.1061/(ASCE)MT.1943-5533.0002160
44. Karki P, Kim YR, Little DN (2015) Dynamic modulus prediction of asphalt concrete mixtures through computational micromechanics. Transp Res Rec 2507(1):1–9. https://doi.org/10.3141/2507-01
45. TL Asphalt-StB 07. (2013). "Technische Lieferbedingung für Asphaltmischgut für den Bau von Verkehrsflächenbefestigung. FGSV Verlag." (In German)
46. EN 12591 (2015) Bitumen and bituminous binders. Specifications for paving grade bitumens. European Committee for Standardization
47. Wistuba M (2016) The German segmented steel roller compaction method–state-of-the-art report. Int J Pavement Eng 17(1):81–86. https://doi.org/10.1080/10298436.2014.925555
48. Zollinger CJ (2005) Application of surface energy measurements to evaluate moisture susceptibility of asphalt and aggregates. Ph.D. Thesis. Texas A&M University, College Station, USA
49. Arand W, Renken P (1990) Entwicklung eines im Laboratorium anwendbaren Verdichtungsverfahrens, durch welches Walzasphalten dieselben mechanischen Eigenschaften wie bei der Walzverdichtung in der Praxis vermittelt werden. Schlussbericht, FE, 7. [in German]
50. Renken P (2001) "Vergleich der mechanischen Eigenschaften von mittels Walz-Sektor-Verdichtungsgerät und Lamellen-Verdichtungsgerät hergestellten Asphaltprobeplatten." Forsch Strassenbau U Strassenverkehrstech, (821). [in German]
51. Yang S, Braham A, Underwood S et al (2017) Correlating field performance to laboratory dynamic modulus from indirect tension and torsion bar. Road Mater Pavement Des 18(sup1):104–127. https://doi.org/10.1080/14680629.2016.1267438
52. Büchler S, Cannone Falchetto A, Walther A et al (2018) Wearing course mixtures prepared with high reclaimed asphalt pavement content modified by rejuvenators. Transp Res Rec 2672(28):96–106. https://doi.org/10.1177/0361198118773193
53. Wang D, Riccardi C, Jafari B et al (2021) Investigation on the effect of high amount of Re-recycled RAP with Warm mix asphalt (WMA) technology. Constr Build Mater 312:125395. https://doi.org/10.1016/j.conbuildmat.2021.125395
54. ASTM D1188–07 (2015) Standard test method for bulk specific gravity and density of compacted bituminous mixtures using coated samples. American Society for Testing and Materials
55. Moon KH, Cannone Falchetto A, Park JY et al (2014) Development of high performance asphalt mastic using fine taconite filler. KSCE J Civ Eng 18(6):1679–1687. https://doi.org/10.1007/s12205-014-1207-6
56. Marasteanu MO, Velasquez R, Cannone Falchetto A et al (2009) Development of a simple test to determine the low temperature creep compliance of Asphalt mixtures. Final Report for Highway IDEA Project 133. Transportation Research Board, Washington, DC
57. Marasteanu M, Buttlar W, Bahia H et al (2012) Investigation of low temperature cracking in asphalt pavements national pooled fund study–phase II.
58. Huet C (1963) Etude par une méthode d'impédance du comportement viscoélastique des matériaux hydrocarbonés. Ph.D. Thesis. Faculté des Sciences de l'Université de Paris, Paris, France [In French]
59. Velasquez RA (2009) On the representative volume element of asphalt concrete with applications to low temperature. Ph.D. Thesis. University of Minnesota, Twin Cities, Minneapolis, USA
60. Yu J, Zhang X, Xiong C (2017) A methodology for evaluating microsurfacing treatment on asphalt pavement based on grey system models and grey rational degree theory. Constr Build Mater 150:214–226. https://doi.org/10.1016/j.conbuildmat.2017.05.181
61. Zhang DB, Li X, Zhang Y et al (2019) Prediction method of asphalt pavement performance and corrosion based on grey system theory. Int J Corros 2019:1–9. https://doi.org/10.1155/2019/2534794

Publisher's Note